



CHORUS

This is the accepted manuscript made available via CHORUS. The article has been published as:

Identification of two mechanisms for current production in a biharmonic flashing electron ratchet

Bryan Lau, Ofer Kedem, Mark A. Ratner, and Emily A. Weiss

Phys. Rev. E **93**, 062128 — Published 20 June 2016

DOI: [10.1103/PhysRevE.93.062128](https://doi.org/10.1103/PhysRevE.93.062128)

Identification of Two Mechanisms for Current Production in a Biharmonic Flashing Electron Ratchet

Bryan Lau^{1,2}, Ofer Kedem², Mark A. Ratner^{1,2}, and Emily A. Weiss*^{1,2}

¹ *Department of Chemistry, Northwestern University, 2145 Sheridan Rd., Evanston, IL 60208-3113*

² *Center for Bio-Inspired Energy Science, Northwestern University, 303 E. Superior Street, 11th floor, Chicago, Illinois 60611-3015*

*corresponding author. Email: e-weiss@northwestern.edu

CLASSIFICATION: Physical sciences, Chemistry

KEYWORDS: Electron transport, Non-equilibrium, Flashing ratchet, Quantum Dynamics

Abstract: Ratchets rectify the motion of randomly moving particles, which are driven by isotropic sources of energy like thermal and chemical energy, without applying a net, time-averaged force between source and drain. This paper describes the behavior of a damped electron, modeled by a quantum Lindblad master equation, within a flashing ratchet (a one-dimensional potential that oscillates between a flat surface and a periodic asymmetric surface). By examining the complete space of all biharmonic potential shapes and a large range of oscillation frequencies, two modes of ratchet operation, differentiated by their oscillation frequencies (relative to the rate of electron relaxation), are identified. Slow-oscillating, strong friction ratchets operate by a classical, overdamped mechanism. In fast-oscillating, weak friction ratchets, current is primarily produced when the frequency of the oscillating potential is resonant with the beating of the electron wavefunction in the potential well. The shape of the ratchet potential determines the direction of the current (and, in some cases, straightforwardly accounts for current reversals), but the maximum achievable current at any shape is controlled by the degree of friction applied to the electron.

INTRODUCTION

A ratchet is a non-equilibrium scheme that rectifies the motion of randomly moving particles without a net applied force in the direction of transport, by breaking symmetries of the particle motion in space and time. Ratcheting is the operative mechanism of biological enzymes, pumps, and motors [1,2], and has been experimentally realized in particle separators and sorters [3-8]. In particular, a “flashing” ratchet works by switching, continuously or instantaneously, between two states of the potential surface on which the particle travels (**Figure 1a**): (i) a surface with periodic features that are asymmetric in the direction of transport, and (ii) a surface that allows random, isotropic diffusion of a particle (*i.e.*, a flat potential). The random motion of the particle, due to its coupling to the environment, is rectified by the local, time-dependent forces from the oscillating potential. An exciting possible application of such a mechanism is the enhancement of directional transport in nanostructured organic and inorganic materials by ratcheting the charge carriers [9,10]. In photovoltaic, sensing, logic, and low power devices based on these materials, electron motion is randomized by strong electron-phonon coupling and an abundance of scattering mechanisms, which lead to fast dissipation of electronic energy into the vibrational bath. A method to induce transport of highly damped charge carriers toward the current-collecting electrodes by rectifying their random thermal motion is therefore a promising avenue for improving the performance of these devices. A flashing electron ratchet (as we model here) [11-13] – as opposed to a tilting ratchet, where the asymmetric potential is rocked by an oscillating force – is particularly suited to improving the yield of charge collection in photovoltaic and sensing devices, because it introduces the oscillating potential through a gate electrode, rather than requiring the application of an alternating source-drain bias [14] or scattering features [15-18] that could interfere with the collection of current.

In this work, we study the mechanisms by which a simple model of a flashing ratchet, in which a damped electron travels along one dimension within an oscillating biharmonic potential, achieves directional current without applied bias. The local spatial symmetry is broken by the asymmetric features of the periodic potential, and the temporal symmetry is broken through coupling the electron to the environment *via* a Lindblad master equation, a purely quantum mechanical propagator. Although a very short electronic dephasing lifetime (1-100 fs over distances of 1 – 10 nm) ensures that coherence does not play a role in electron transport in this system, the use of a quantum propagator properly describes the electron’s behavior at nanometer

length scales by allowing for tunneling during certain portions of the potential's oscillation period. In a flashing ratchet potential, there is no net bias. Significant tunneling therefore leads to the formation of a delocalized state where the electron no longer feels the local asymmetry of the potential. Tunneling therefore decreases the ratchet current from that achieved by a purely classical system. In contrast, a tilting ratchet preserves the asymmetry of the potential because the applied bias changes the potential depending on the direction of the tilt [14,19]. We explore the parameter space of all possible biharmonic shapes, by far the most common set of asymmetric potentials used in the literature [5,20,21], and a large range of oscillation frequencies for the potential, and study the influence of these parameters on the net directional current achieved by the ratcheting mechanism. This work represents the first systematic study of the effect of potential shape on the current produced in a flashing electron ratchet with a quantum mechanical propagator.

Our most important finding is that there exist two distinct modes of ratcheting, characterized by the ratio of the potential oscillation timescale to the electron relaxation timescale (i.e., the degree of friction applied to the electron). “Fast” electron ratchets, where the potential oscillation and relaxation timescales are similar, exploit resonances between the oscillation of the potential and the damped beating of the electron wavefunction inside a potential well to maximize directional current. “Slow” electron ratchets operate like classical, overdamped ratchets (see **Figure 1a**). The shape of the ratchet potential determines, at least in the case of slow ratchets, the direction of the current, and accounts for often mysterious “current reversals” that can manifest upon variations of any ratchet parameter [20]. The maximum magnitude of the current achievable by the ratchet for any biharmonic shape is controlled by the degree of friction applied to the electron; fast ratchets achieve a globally higher maximum current than slow ratchets.

The current in flashing ratchets is sensitive to the variation of any parameter, including friction, driving amplitude, frequency, and temperature [20,22]. Recent computing advances have enabled studies that show that the ratchet current is a deeply complex function of large, combined parameter spaces [23-27], but physical intuition on many characteristics of flashing ratchets, including current reversals and resonances, remains sparse. Here, we identify two parameters, the shape of the potential and the amount of friction on the electron (defined as the ratio of the potential oscillation timescale to the electron relaxation timescale), that, when explored simultaneously over a large parameter space, reveal two modes of ratchet operation that

produce current by two different mechanisms. Prior work that explored the effect of shape on the behavior of the ratchet current focused on variations to a single potential [28-34]; however, while the current from a ratchet of a single shape does show resonances at certain oscillation frequencies [20], examining the frequency dependence of a single shape does not make apparent the transition from under-damped to over-damped ratcheting mechanisms. Identifying this transition, which is only possible when considering the complete space of biharmonic shapes and a large range of friction values, is critical in uncovering physically intuitive behaviors, and relating these behaviors to structural features of this complex system.

Description of the Model. *The Lindblad Master Equation.* We consider the dynamics of a single (non-interacting) damped electron moving in a one-dimensional potential that is periodic in space and time. Our electron is not a wavepacket moving within a lattice; it is an electron with a periodic wavefunction within a periodic potential. The damping is induced by Ohmic coupling of the electron to a large number of harmonic oscillators at some temperature, T , such that the bath always remains in thermal equilibrium (Born-Markov approximation). By eliminating the bath degrees of freedom, implicit effects of the bath are left on the electron, namely decoherence and dissipation [35-38]. The Lindblad master equation (LME) that we choose is given in eq 1 (in atomic units). In eq 1, ρ

$$\frac{\partial \rho}{\partial t} = -i[H_S, \rho] - i\gamma_0[x, \{p, \rho\}] - 2m_e\gamma_0k_B T[x, [x, \rho]] - \frac{\gamma_0}{8m_e k_B T}[p, [p, \rho]] \quad (1)$$

is the density matrix in the Schrodinger picture, H_S is the system Hamiltonian, γ_0 is the system-bath coupling, m_e is the effective mass of the electron, k_B is Boltzmann's constant, and $\{p, \rho\}$ is an anti-commutator. The first term on the RHS is the non-dissipative Liouville von-Neumann term. The second and third terms, respectively, describe momentum damping (dissipation) and localization (decoherence). The fourth term guarantees positivity of the density matrix at all times; without this term, eq 1 is the Caldeira-Leggett master equation. This particular form of the LME yields translationally-invariant relaxation and allows us to control the relaxation with just two parameters, γ_0 and T .

For the specific form of the LME in eq 1, the coupling strength γ_0 to the bath causes an exponential decay of the momentum p (and thus energy) in time [38]: $\langle \hat{p} \rangle_t \propto \langle \hat{p} \rangle_0 e^{-2\gamma_0 t}$. We choose γ_0 to yield a momentum half-life $\tau_{relax} = \frac{\ln(2)}{2\gamma_0} = 50 \text{ fs}$. We will see later that it is the

ratio of τ_{relax} to the oscillation period, rather than the absolute value of τ_{relax} , that influences the ratchet current.

The decay of spatial coherence is governed by the third term on the RHS of eq 1, which suppresses the off-diagonal elements of the density matrix [38]: $\rho(x, x', t) = \rho(x, x', 0)e^{-2m_e\gamma_0k_B T(x-x')^2 t}$, where x and x' are two different positions within the 1D ratchet potential. Since the master equation we use is derived for a non-periodic potential, the rate of this decoherence process grows, without bound, with increasing separation between two positions. Within the periodic ratchet potential, however, $\psi(x+L) = \psi(x)$, so the maximum distance between x' and x is $L/2$. We therefore modify the distance matrix $(x-x')$ by subtracting L from any $(x-x') > L/2$ and adding L to any $(x-x') < -L/2$. With this modification, eq 1 respects the periodic boundary conditions of the ratchet potential.

Initial Conditions. The initial state of the electron is a thermally-weighted sum of the eigenfunctions of the system, eq 2, where $\beta = \frac{1}{k_B T}$ is the inverse temperature, $Z = Tr(e^{-\beta H})$

$$\rho_0 = \frac{1}{Z} \sum_n e^{-\beta E_n} |\psi_n\rangle\langle\psi_n| \quad (2)$$

is the quantum partition function, and $|\psi_n\rangle$ is an eigenfunction of the system Hamiltonian. Although we can achieve the same steady-state by starting with a symmetric (zero-mean velocity) set of plane waves or wavepackets (Figure S1a,b in the Supplemental Material [39]), eq 2 allows the system to achieve a steady state with the least computational effort. The temperature of the system at $t = 0$ and the temperature of the bath are set to 300 K. The temperature of the bath influences the final equilibrium state and the decoherence rate, but since the decoherence rate is much faster than the dissipation rate, and the system is designed such that the thermal equilibrium is never achieved, the effect of the exact temperature on the steady-state mean velocity of the electron is minimal (Figure S1c,d in the Supplemental Material [39]).

The Form of the Ratchet Potential. The ratchet potential is represented as a biharmonic Fourier series (**Figure 1b,c**), eq 3, where L is the spatial period of the ratchet potential, and a_n

$$V(x, t) = \sin^2\left(\frac{\pi t}{\tau_{ratchet}}\right) \left[a_1 \sin\left(\frac{2\pi x}{L}\right) + a_2 \sin\left(\frac{4\pi x}{L}\right) \right] \quad (3)$$

are the coefficients (in units of energy, eV) of the Fourier terms; the range $0 \leq a_1, a_2 \leq 4.5$ eV is chosen to capture a large set of confining potentials for an electron with an initial kinetic energy of 25 meV (i.e. 300 K). The spatial period L is set to 50 nm, similar to the length scale of

state-of-the-art photolithographic patterning techniques. Since L is much greater than the length-scale of atomic potentials, we assume that the electron travels in a parabolic conduction band with effective mass $m_e = 1$, *i.e.*, a free or nearly-free particle, with no static disorder. Our conclusions about the general behaviors of biharmonic electron ratchets, including the presence of two ratcheting regimes at different levels of friction, do not depend on the absolute value of the ratchet spatial period, bath temperature, or coupling constant, as our equation of motion (eq 1) can be written in dimensionless form (see the Appendix). In the Supplemental Material [39], we show two sets of results where we use different values for L and γ_0 than in the main text.

We vary the oscillation period of the ratchet, $\tau_{ratchet}$, about the momentum relaxation half-life τ_{relax} (50 fs, eq 1). For each ratio $\frac{\tau_{ratchet}}{\tau_{relax}}$, we calculate the steady state velocity of the electron $\langle\langle v \rangle\rangle$, where the first set of brackets denotes the quantum expectation value, and the second set of brackets denotes a time average over one oscillation period of the potential, as a function of a_1 and a_2 . The mean velocity is directly proportional to the current, and we use the two terms interchangeably.

The density matrix of the electron is represented in the Fourier grid basis [40] with 256 grid points, and propagated according to eq 1, for 2.5 ps or ten oscillation periods, whichever is greater, using the variable order Adams-Bashforth-Moulton predictor-corrector algorithm in MATLAB (ode113). We explicitly simulate only one period L of the ratchet potential, with periodic boundary conditions. Since the coherence length of the electron (as given by its thermal wavelength $\lambda = \frac{1}{\sqrt{2m_e k_B T}} \sim 1.9 \text{ nm}$) is much smaller than the period, L , of the potential, self-interference is negligible due to the fast decoherence rate as well as the localized behavior of the wavefunction, as shown in the supplementary movies (for example, the latter half of Movies M1 and M2).

RESULTS AND DISCUSSION

Figure 2 is a series of color maps of the non-equilibrium steady-state velocity of the electron, $\langle\langle v \rangle\rangle$, as a function of the Fourier coefficients a_1 and a_2 , for a series of ratios $\frac{\tau_{ratchet}}{\tau_{relax}}$. Figure S2 in the Supplemental Material [39] contains the full dataset that we calculated (*i.e.*, plots for more values of $\frac{\tau_{ratchet}}{\tau_{relax}}$). Positive current is shown in shades of red and yellow, and negative current is shown in shades of blue and purple. A generic, symmetric color bar is shown at the top of the

figure; the actual range of $\langle\langle v \rangle\rangle$ represented by that color bar changes from tile to tile in order to best visualize the features of each plot. **Figure 3** shows the maximum value of $\langle\langle v \rangle\rangle$ versus the timescale ratio $\frac{\tau_{ratchet}}{\tau_{relax}}$. In every case, the maximum value of $\langle\langle v \rangle\rangle$ is positive for reasons we discuss below.

The amplitude of the ratchet potential at any given time depends on the absolute values of a_1 and a_2 , but the ratio of the Fourier coefficients $\frac{a_2}{a_1}$ determines the shape of the ratchet potential, see **Figure 1b,c**. Any straight line drawn on a plot in **Figure 2** that goes through the origin traces out a series of potentials with the same shape. For example, the dotted lines corresponding to $\frac{a_2}{a_1} = 0.25$ represent the widely studied biharmonic approximation to the piecewise linear sawtooth ratchet potential, which is chosen as a “typical example” of a ratchet potential [20]. By inspection of the plots in **Figure 2**, we see that, in fact, the peak currents as a function of the ratchet shapes we study here, at least those with $\frac{\tau_{ratchet}}{\tau_{relax}} > 1$, tend to fall on the line with $a_2 \sim 0.6a_1$ (shown as dashed lines on the plots in **Figure 2**). When a_1 or a_2 is equal to zero (along the x and y -axes of the plots in **Figure 2**) the potential is symmetric, and $\langle\langle v \rangle\rangle$ is zero within machine precision.

The parameter $\tau_{ratchet}$ (eq 3) is a measure of the rate at which the electron periodically receives energy from the ratchet potential, and τ_{relax} (eq 1) is a measure of the rate at which the electron loses energy to the environment. **Figure 3** shows a plot of the maximum velocity $\langle\langle v \rangle\rangle$ at each timescale ratio, $\frac{\tau_{ratchet}}{\tau_{relax}}$, chosen from all possible biharmonic shapes. This plot has two peaks, at $\frac{\tau_{ratchet}}{\tau_{relax}} \sim 1$ and ~ 20 , separated by an inflection point at $\frac{\tau_{ratchet}}{\tau_{relax}} \sim 3$. We colloquially refer to the ratchets with $\frac{\tau_{ratchet}}{\tau_{relax}} < 3$ as “fast” ratchets, and ratchets with $\frac{\tau_{ratchet}}{\tau_{relax}} > 3$ as “slow” ratchets. The timescale ratio that produces the global maximum of $\langle\langle v \rangle\rangle$ is ~ 1 ; if the ratio is not ~ 1 , changing the shape of the potential (by changing a_1 or a_2) cannot increase the velocity to the global maximum. The Supplemental Material [39] shows that these two regimes of ratcheting are also distinguishable for ratchets with different values of for $\tau_{ratchet}$ (Figure S3) and L (Figure S4), although we do not necessarily observe a peak in $\langle\langle v \rangle\rangle$ as a function of $\frac{\tau_{ratchet}}{\tau_{relax}}$ for slow ratchets.

Mechanisms of Operation for Fast and Slow Ratchets. Our simulations of the behavior of the electron in the ratchet potential, shown in the movies in the Supplemental Material [39], allow us to understand the bimodal dependence of $\langle\langle v \rangle\rangle$ on $\frac{\tau_{ratchet}}{\tau_{relax}}$ in **Figure 3**. Slow ratchets operate like classical, overdamped flashing ratchets, as seen in **Figure 1a**. The wavefunction spreads as the potential turns off; as the potential turns on again, it causes an asymmetric relaxation, and ratchet current results, see Movie M1. If the oscillation of the potential becomes too slow, the wavefunction fully delocalizes before the ratchet potential turns on again, and no current results. Additionally, in the limit $\frac{\tau_{ratchet}}{\tau_{relax}} \gg 1$ the electron remains in the equilibrium state of the instantaneous potential, and no current results, see Figure S5 in the Supplemental Material [39].

In “fast” ratchets ($\frac{\tau_{ratchet}}{\tau_{relax}} \sim 1$), the oscillating potential exerts a high impulse ($I = - \int_t^{t+\tau_{ratchet}} \frac{dV}{dx} dt$) on the electron. Under these conditions, the rate of energy input exceeds the relaxation rate, and the electron undergoes damped beating inside the wells, see Movie M2 (1:00 min and onwards). If the beating is resonant with the oscillation frequency of the potential (or integer multiples of that oscillation frequency), then the potential turns off as the wavefunction spreads, such that the wavefunction releases two wavepackets travelling in opposite directions. As the potential turns on again, if the potential surface is sufficiently asymmetric, one wavepacket moves to the adjacent well, while the second one is reflected back to the original well. Eventually, a localized, right-moving wavepacket redevelops and is resonantly accelerated by the oscillating potential. This mechanism leads to net unidirectional acceleration of the wavefunction and ratchet current. If, however, the beating is out of phase with the oscillations of the potential, then the wavefunction is contracting as the potential turns off, and no current results, see Movie M3. Furthermore, in the limit of very fast oscillations ($\frac{\tau_{ratchet}}{\tau_{relax}} \ll 1$), which is quickly approached on the left side of the plot in **Figure 3**, the electron sees an averaged, static potential, and no current is produced, see Figure S6 in the Supplemental Material [39].

The resonances between the oscillating potential and the beating wavepacket appear in plots of $\langle\langle v \rangle\rangle$ versus the oscillation period for a given potential shape (some examples are in **Figure 4a**). Resonant behavior due to vibrations of a particle inside a potential well have been observed

in classical flashing ratchets where the particle has finite inertia, i.e., is not overdamped [41,42], because the equations of motion for overdamped particles have no inertial term that allows for beating or other non-equilibrium dynamics. This mechanism is therefore only operative for “fast” or weak friction ratchets, and not for “slow” or strong friction ratchets. We note that the mechanism for the resonances in current we observe here is distinct from the phase coherence that produces current in some quantum ratchet systems [43-48].

Since a given potential can induce wavefunction beating that is resonant with the oscillation frequency of the potential, we also expect that a given oscillation frequency will be resonant with the beating of the wavefunction within different potential shapes. These “resonant shapes” manifest as the interference pattern-like features in the plots in **Figure 2**; these patterns are most clearly apparent for $2.18 < \frac{\tau_{ratchet}}{\tau_{relax}} < 4.84$, but exist up to $\frac{\tau_{ratchet}}{\tau_{relax}} < 9.67$. The tilted bands of high current are separated by regions where the average velocity is a factor of $10^2 - 10^4$ lower than the current in those bands. The bands of current in **Figure 2** are approximately vertical rather than horizontal because fixing the value of a_2 and varying a_1 increases the asymmetry while preserving the general shape of the potential, whereas fixing a_1 and varying a_2 changes the shape of the potential *and* its asymmetry, **Figure 1b,c**.

To simulate the interference pattern-like features, let us assume that the electron spends most of its time in the deepest wells of the periodic ratchet potential, and calculate its damped, natural frequency ω_D from its energy in one period of the static potential $V(x) = a_1 \sin\left(\frac{2\pi x}{L}\right) + a_2 \sin\left(\frac{4\pi x}{L}\right)$, using the harmonic approximation $\langle\langle E \rangle\rangle = \hbar\omega_D$ (the minimum of the potential is deep enough so that the ground state is localized). A numerical solution for the ground state, as opposed to evaluating $m\omega_{bare}^2 = \left.\frac{\partial^2 V}{\partial^2 x}\right|_{x_0}$, is needed for even qualitative accuracy as it takes into account the relaxation from the bath. We plot $\omega_D = \frac{1}{\tau_D}$ as a function of a_1 and a_2 in **Figure 4b**. We then multiply every value in that plot by, for example, $\tau_{ratchet} = 48 \text{ fs}$ ($\frac{\tau_{ratchet}}{\tau_{relax}} = 0.967$) such that each point now corresponds to the ratio $\tau_{ratchet}/\tau_D$. Finally, we color integer multiples of $\tau_{ratchet}/\tau_D$ (and values that are within ± 0.1 of integer multiples) red to obtain the tilted vertical stripe pattern shown in the inset of **Figure 4b**. Within these stripes, the oscillation of the potential is synchronized (i.e., an integer multiple) with the beating of the wavefunction, which is the source of the resonant peaks in velocity shown in **Figure 4a** and **Figure 2**. For increasing

values of $\tau_{ratchet}$, the number of values of ω_D that are integer multiples of $1/\tau_{ratchet}$ in the space of potential shapes that we examine increases, so the number of bands that fit into the plots in **Figure 2** increases. The vertical columns in the inset of **Figure 4b** do not line up exactly with the features in **Figure 2**, because ω_D is calculated for a static potential whereas the ratchet is time-dependent, and because the harmonic approximation only considers the curvature of the potential well at its minimum.

As $\frac{\tau_{ratchet}}{\tau_{relax}}$ (i.e. friction) increases, the bands of current in the plots in **Figure 2** begin to blend together. The resonance condition is weakening because the increasing friction damps the beating of the wavefunction before the potential goes through one oscillation cycle. We observe a local minimum in ratchet current at $\frac{\tau_{ratchet}}{\tau_{relax}} \sim 3$, **Figure 3**, because the oscillation is too slow to exploit the beating of the wavefunction before it is damped, and too fast to allow the wavefunction to spread. As the ratchet slows further, the impulse from the potential decreases, and high-barrier potentials (which, for fast ratchets, provided the high impulse that induced beating of the wavefunction) now trap the electron. The peak current therefore moves toward lower-magnitude potentials (i.e., the origins of the plots in **Figure 2**), and the current decreases monotonically outward from the origin, along lines of constant shape $\frac{a_2}{a_1}$. We confirmed that the interference pattern-like features are not present in plots for the slowest (high friction) ratchets by conducting a parameter sweep for $\frac{\tau_{ratchet}}{\tau_{relax}} = 12.1$ and $0 \leq a_1, a_2 \leq 1.5 \text{ eV}$ at three times the energy resolution used to construct the plots in **Figure 2**; these calculations did not reveal any new features.

The Scaling Relationship between Current Maps. For the set of fast ratchets where $\frac{\tau_{ratchet}}{\tau_{relax}} < 2.42$, as $\frac{\tau_{ratchet}}{\tau_{relax}}$ decreases it appears that we are zooming in on the features in the plot $\frac{\tau_{ratchet}}{\tau_{relax}} = 2.42$ in **Figure 2**, such that the striped pattern is eventually no longer apparent. This behavior suggests that there is a scaling relationship among the current maps in **Figure 2**; specifically, the overall structure of the velocity map as a function of the *scaled* coordinates $a'_1 = \tau_{ratchet} a_1$ and $a'_2 = \tau_{ratchet} a_2$ is the same for any fast ratchet. Physically, this result implies that all fast ratchets have the same relationship between the ratchet current and the shape of the potential. But as we pointed out in the discussion of **Figure 3**, the absolute magnitude of

the current is still controlled by the degree of friction applied to the electron – that is, the value of $\frac{\tau_{ratchet}}{\tau_{relax}}$. Animation A1 shows this scaling behavior in the Supplemental Material [39].

For $\frac{\tau_{ratchet}}{\tau_{relax}} < 0.846$, we do not explore a large enough space (a_1, a_2) to record the peak current, so we observe noise in the plot of $\langle\langle v \rangle\rangle$ vs. $\frac{\tau_{ratchet}}{\tau_{relax}}$, **Figure 3**. Extending the upper limit for a_1 and a_2 to 9 eV (from the original 4.5 eV) zooms out and gets closer to the peak current (see red triangles on **Figure 3**). Further increasing a_1 and a_2 to zoom out to the full plot near $\frac{\tau_{ratchet}}{\tau_{relax}} = 2.42$ however makes the potential too confining and limits the maximum achievable current.

Current Reversals in Overdamped Ratchets. For $\frac{\tau_{ratchet}}{\tau_{relax}} > 2.42$ the plots in **Figure 2** are, in general, organized into regions of positive current (upper left region in each plot) and negative current (lower right) separated by the line $a_2 \approx 0.7a_1$. The sign of the current in our ratchet model is determined by the direction of the asymmetry of the potential, shown for three general cases in **Figure 5**. For $a_2 \leq 0.5a_1$ (upper left region of each plot in **Figure 2**), each repeat unit of the potential has one well and one peak (with a shoulder); the asymmetry in this class of structures originates from the different distances from the bottom of the well to its two neighboring peaks, **Figure 5a**. In these structures, the current flows from the well to the closer peak, which, in our potentials, is always to the positive side (right). For $a_2 \geq 0.5a_1$ (lower right region in **Figure 2**), the asymmetric shoulder deepens into a secondary well and peak, **Figure 5b,c**. The change in the sign of the current from positive to negative coincides with the depth of the secondary well becoming greater than the average kinetic energy of the electron, see Figure S7 and Movies M4 in the Supplemental Material [39]. Since the electron can be trapped by the secondary well from its starting point in the deepest well, the asymmetry in the potential is now due to the difference in heights, instead of distances, to the two adjacent peaks, **Figure 5c**. The spreading of an electron wavefunction in the deepest well is less impeded by the lower peak to the left, so the direction of ratchet current in these structures reverses. This flow of negative current is, however, countered by the tendency of probability density, once in the secondary well, to flow in the direction of the lower peak back to the deepest well. The peak current in the negative direction is therefore always smaller than the peak current in the positive direction, and thus the global maximum in current for a given ratio $\frac{\tau_{ratchet}}{\tau_{relax}}$ is always positive, **Figure 3**. This

mechanism does not entirely explain current reversals for fast ratchets, which we are still investigating. Current reversals as a function of shape have been observed in “delta-kicked” ratchet models [24]; however, the mechanism we describe here depends on the ratchet potential trapping the dynamically relaxing wavefunction, a feature that is absent in a delta-kicked model since the potential is only on during the instantaneous kick.

CONCLUSIONS

In summary, we constructed a quantum model of an electron in a flashing ratchet potential. The electron experiences dissipation and decoherence through a Lindblad master equation. We calculated the average steady-state velocity of the electron in all possible biharmonic shapes and large range of oscillation frequencies of the potential (**Figure 2**). We find that the ratio of timescales of oscillation of the potential and dissipation of the electron, $\frac{\tau_{ratchet}}{\tau_{relax}}$ (i.e., the friction on the electron) is the most important parameter in determining the magnitude of the ratchet current, **Figure 3**. Furthermore, we observe two distinct modes of ratchet operation. Weak-friction ratchets, $\frac{\tau_{ratchet}}{\tau_{relax}} < 3$, achieve higher currents than strong-friction (heavily-damped) ratchets, by exploiting resonances between the non-equilibrium beating of the wavefunction inside the potential wells and the oscillation of the potential. For strong-friction ratchets, reversals of current (from positive to negative) in shape space are related intuitively to the type of asymmetry present in the potential, **Figure 5**. The timescale ratio $\frac{\tau_{ratchet}}{\tau_{relax}}$ can be expressed as a combination of multiple sub-relaxation timescales, including relaxation of the electron in-well and transmission between barriers, as investigated by Tarlie and Astumian [49], who use a potential that switches instantaneously between static “on” and “off” states, but these quantities are difficult to deconvolve for a continuously driven system like the one we describe here.

Quantifying the importance of quantum effects in our model is not straightforward, but we can make the following two comments. First, the decoherence lifetime in our system is too fast for quantum coherences to be contributing to transport in any way. Second, our system is certainly different from one propagated classically (using, for example, the Langevin equation), because a quantum equation of motion, even in the fast decoherence limit, allows for tunneling. Since tunneling through a flashing barrier has the same transmission probability regardless of direction, it is an isotropic mechanism of transport that reduces the overall efficiency of the

ratchet by randomizing electron motion, see Movie M5. The quantum master equation is essential to revealing that tunneling in a flashing ratchet lowers the current, as opposed to a tilting ratchet [19], where a rocking potential changes the tunneling transmission probability depending on the incident direction, although tunneling can also decrease the current [50]. Flashing ratchets that produce the most current therefore tend to be very confining: the ratio of the amplitude of optimal potentials to the steady-state kinetic energy of the electron ranges from three for fast ratchets to over thirty for slow ratchets. Due to the height and width of the potential barriers, any probability density that is inside classically forbidden regions as the potential turns on is reflected in the classical direction, and the amount of tunneling between wells is negligible. We do observe that wave-like behavior of the electron, such as the beating of the wavefunction seen in fast ratchets, is essential to producing current; this type of resonance is also, however, present in classical particle ratchets under certain conditions. We are currently building a classical equivalent of our model to quantitatively explore the effect of quantum transport on the ratchet current.

Finally, we note that in **Figure 2** increasing $\frac{\tau_{ratchet}}{\tau_{relax}}$, i.e., increasing the friction on the electron, decreases the sensitivity of the current to the biharmonic shape. In fact, in the overdamped limit that is a common starting point for many models, our calculations show negligible dependence of ratchet behavior on shape, so only studying a single potential shape may be appropriate. A similar decrease in the sensitivity of ratchet performance to shape in the high damping and/or weak-kick limit has been seen for delta-kicked ratchets [23-25]. Our work highlights the importance of searching both shape and frequency space in drawing general conclusions about ratchet behavior beyond the overdamped limit, especially since it appears that ratchets with a larger inertial component perform better than overdamped ratchets under many conditions.

The oscillation frequencies (THz) and length scales (50 nm) we choose here can be realized by using plasmonic nanostructures to concentrate infrared radiation [51]. A periodic array of such structures could be used to enhance transport in a solar cell by capturing otherwise unabsorbed infrared energy. The Supplemental Material [39] shows, however, that our conclusions do hold for other values of the potential period L and bath coupling strength γ_0 . Our ability to write the master equation in dimensionless form (see the Appendix) implies that our conclusions apply, in general, to non-interacting particles with Ohmic dissipation, because

modifying parameters within the dimensionless ratios (such as inserting a specific effective mass or $E(k)$ dispersion) does not introduce any *new* mechanisms of motion. Different forms of the spectral density, which describe the coupling to the bath, can however introduce new timescales of dissipation and decoherence that may lead to quantitatively and qualitatively different results than what we obtain here. We also expect our assumption of non-interacting particles to fail if the Debye screening length is greater than the average inter-electron distance $b = 1/2N_e^{-3}$, where N_e is the local electron concentration, which may be the case when the wavefunction is localized in the wells of the potential [11].

In future work, we will explore higher dimensional Fourier series of periodic potentials, where we will have access to a larger variety of shapes, with more sophisticated search techniques, such as genetic algorithms or simulated annealing, instead of the brute force approach we use here. The fact that the ratchet current is sensitive to the variation of any parameter shows that such large-scale studies of ratchet parameter space are necessary to illuminate general characteristics of ratchets, however physically intuitive or non-intuitive these characteristics may be.

Acknowledgements. We thank Prof. Igal Szleifer, Dr. Andrew Rasmussen and Mohamad Kodaimati for valuable discussion. This work was supported as part of the Center for Bio-Inspired Energy Science (CBES), an Energy Frontier Research Center funded by the U.S. Department of Energy, Office of Science, Basic Energy Sciences under Award #DE-SC0000989.

APPENDIX

The master equation (eq 1) can be written in dimensionless form using the following substitutions:

$$\begin{aligned} x' &= \frac{x}{L} \\ p' &= \frac{p}{mL\gamma_0} \\ t' &= t\gamma_0 \end{aligned} \tag{A1}$$

Yielding the dimensionless master equation and the rescaled kinetic and potential energy operators (in atomic units and without the prime annotation):

$$\frac{\partial \rho}{\partial t} = -\frac{i}{\gamma_0} [H, \rho] - iL^2\gamma_0[x, \{p, \rho\}] - 2m_e kTL^2[x, [x, \rho]] - \frac{m_e L^2 \gamma_0^2}{8kT} [p, [p, \rho]] \tag{A2}$$

$$T = m_e L^2 \gamma_0^2 \frac{p^2}{2}$$

$$V(x, t) = \sin^2\left(\frac{\pi t}{\gamma_0 \tau}\right) [a_1 \sin(2\pi x) + a_2 \sin(4\pi x)]$$

Equation A2 is scale invariant in space because the potential is periodic, hence x' can only vary between $[0,1]$, and is also scale invariant in time due to decoherence and dissipation (in the long time limit, the velocity reaches a steady state). The value of the dimensionless constants in front of the double commutators defines a ratio of the three parameters L , T , and γ_0 (the spatial period, temperature of the environment, and coupling constant to the environment, respectively) that will give the same results for any actual values chosen so long as they are combined in the same ratio.

In the Supplemental Material [39], we show two additional sets of data that lead to different values for the dimensionless constants, and thus two different families of solutions. The same features that we discuss in the main text, namely two regimes of ratcheting, the peak current and resonance features in fast ratchets, and the broad, featureless smears in slow ratchets, remain the same.

FIGURES

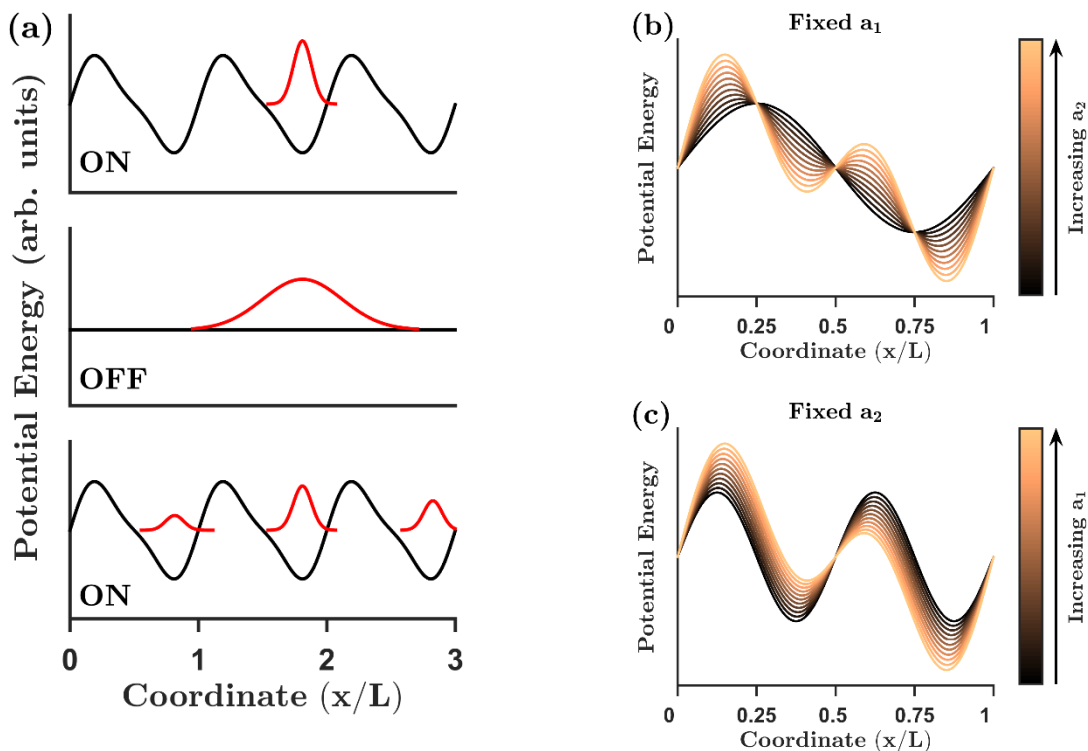


Figure 1. Basic description of the flashing ratchet and ratchet potential. **(a)** An illustration of the general mode of operation of a classical overdamped ratchet. The probability density function (quantum or classical) begins localized in a well. When the potential turns off, the random forces from the bath spread the probability density isotropically. As the potential turns on again, the local, periodic asymmetry of the potential surface causes asymmetric relaxation of the probability density, rectifying the random motion. This mechanism does not work if the switching is much faster or much slower than the characteristic spreading time of the probability density function. Only one period of the ratchet potential is simulated, with periodic boundary conditions, for the results and discussion. **(b,c)** The effect on the shape of the biharmonic potential $V(x) = a_1 \sin\left(\frac{2\pi x}{L}\right) + a_2 \sin\left(\frac{4\pi x}{L}\right)$ of **(b)** fixing the coefficient a_1 while varying a_2 , or **(c)** fixing a_2 while varying a_1 . In **(b)** the degree of asymmetry changes, while in **(c)** the shape is largely preserved but relative heights of the peaks and depths of wells change.

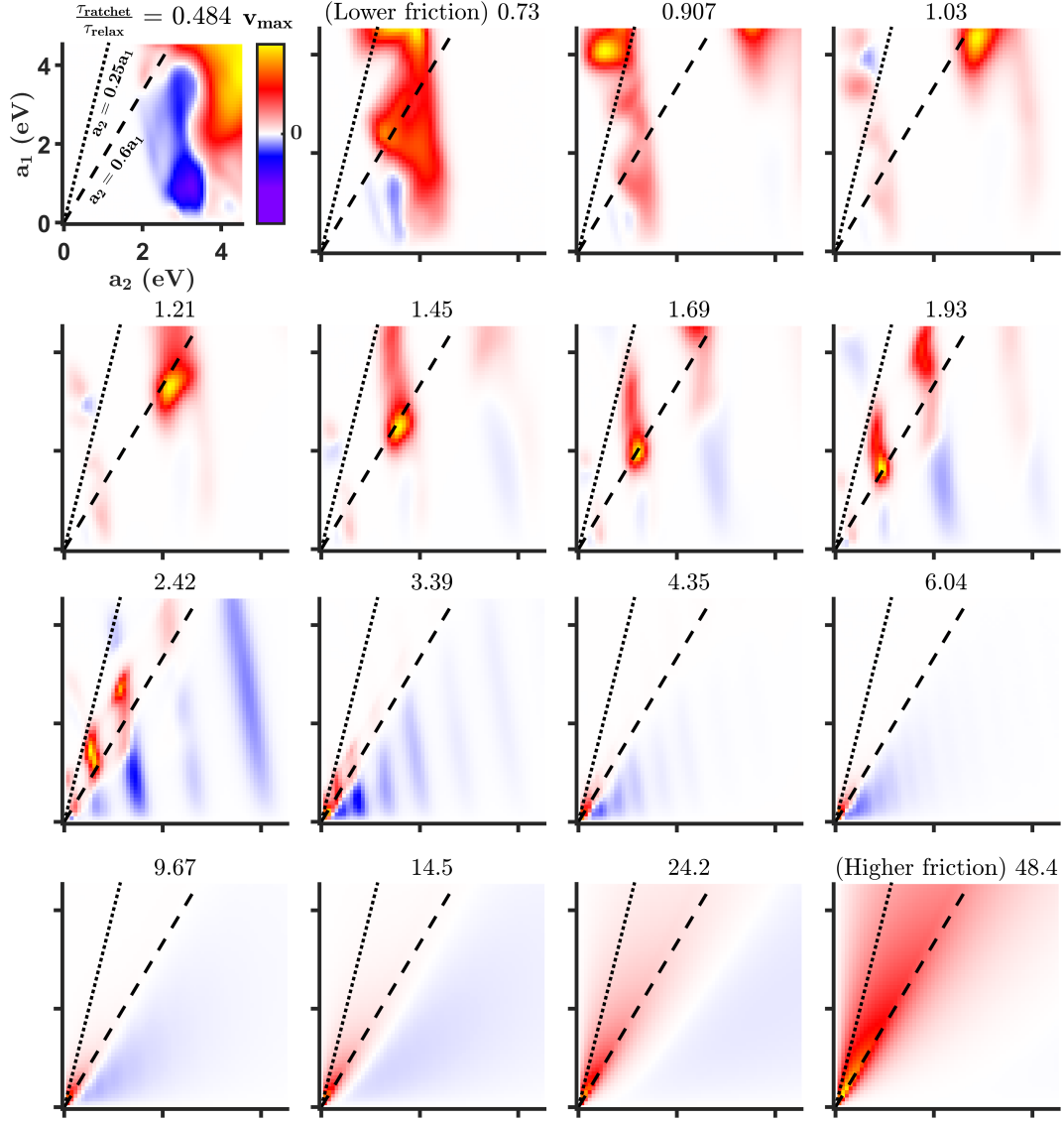


Figure 2. Plots of the average steady-state velocity $\langle\langle v \rangle\rangle$ of the electron as a function of the biharmonic Fourier coefficients a_1 and a_2 , for a series of ratios of oscillation and dissipation time constants, $\frac{\tau_{ratchet}}{\tau_{relax}}$ (where τ_{relax} is constant). All plots comprise 60×60 calculated values of $\langle\langle v \rangle\rangle$ and have the same ranges of values on the x - and y -axes: $0 \leq a_1, a_2, \leq 4.5$ eV. The absolute values of $v_{max} = \max(\langle\langle v \rangle\rangle)$ and $-v_{max}$ (color bar) are different for each plot; the color bar is adjusted from plot to plot to best show the features of the plot. Along lines going through the origin, the ratio $\frac{a_2}{a_1}$, and therefore the shape of the ratchet potential, is constant. The dotted ($a_2 = 0.25a_1$) and dashed ($a_2 = 0.6a_1$) lines correspond to the shape most used in the literature and the shape that we find produces the most current for $\frac{\tau_{ratchet}}{\tau_{relax}} \gtrsim 1$, respectively. The full data set is shown in the Supplemental Material [39].

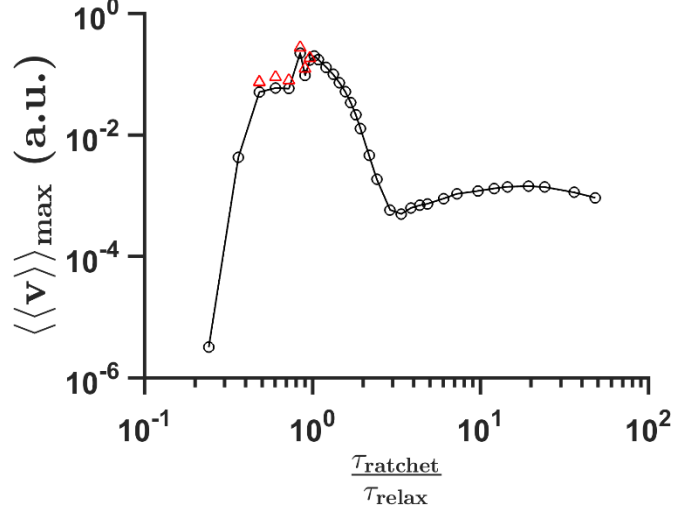


Figure 3. A plot of the maximum average velocity $\langle\langle v \rangle\rangle_{\max}$ of the electron in the parameter space $0 \leq a_1, a_2 \leq 4.5$ eV at each time scale ratio, $\frac{\tau_{\text{ratchet}}}{\tau_{\text{relax}}}$, extracted from the plots in Figure 2. For reasons explained at the end of the text $\langle\langle v \rangle\rangle_{\max}$ is always positive, so $\langle\langle v \rangle\rangle_{\max} = |\langle\langle v \rangle\rangle|_{\max}$. The values of τ_{relax} and of the temperature T of the bath are constant across the data set. There are two distinct peaks in this plot, centered around $\frac{\tau_{\text{ratchet}}}{\tau_{\text{relax}}} \sim 1$ and $\frac{\tau_{\text{ratchet}}}{\tau_{\text{relax}}} \sim 20$. The noise around $\frac{\tau_{\text{ratchet}}}{\tau_{\text{relax}}} \sim 1$ is due to the range of a_1 and a_2 that we explored not being large enough to capture the maximum current; extending the upper range of a_1 and a_2 to 9 eV comes closer to capturing the maximum current (red triangles).

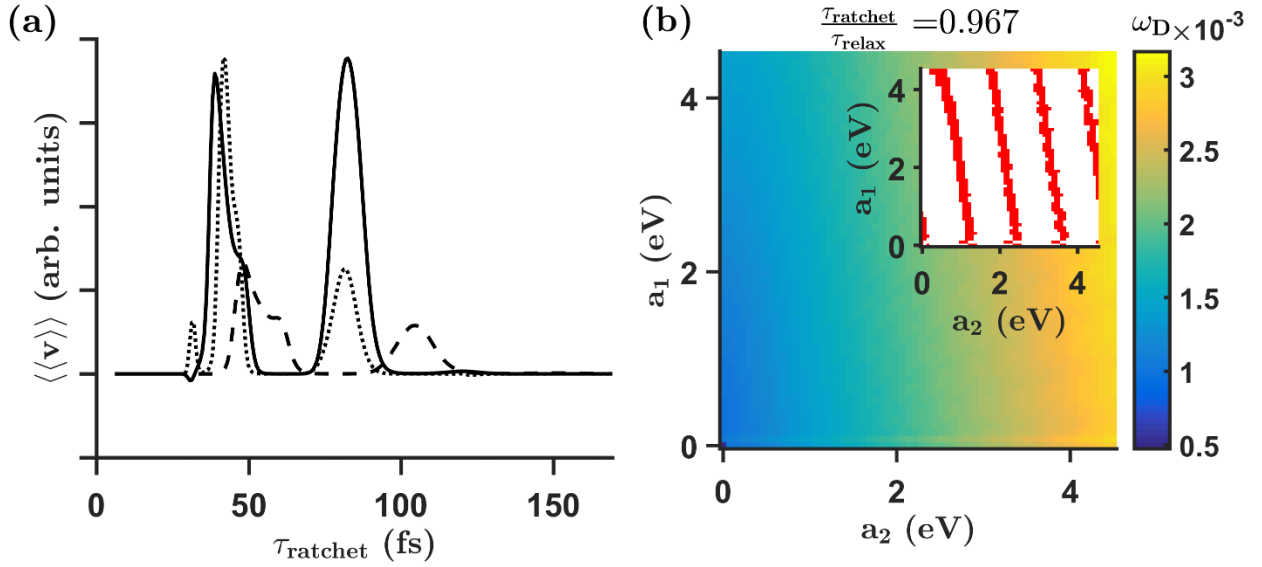


Figure 4. Illustrations of the resonance mechanism for the operation of “fast” flashing ratchets. **(a)** A plot of the average velocity $\langle\langle v \rangle\rangle$ of the electron *versus* the oscillation period of the ratchet potential for three different potential shapes: $(a_1, a_2) = (1.98, 1.21)$ (solid), $(1.44, 0.76)$ (dashed), and $(3.50, 1.06)$ (dotted), in eV. The peaks are a result of resonances between the frequencies of wavefunction beating and potential oscillation. **(b)** A plot of the damped, natural

frequency ω_D of an electron in a *static* potential defined by biharmonic Fourier coefficients a_1 and a_2 , in the harmonic approximation $\langle E \rangle = \hbar\omega_D$. **(Inset):** The result of multiplying the plot in **(b)** by $\tau_{ratchet} = 48 fs$ ($\frac{\tau_{ratchet}}{\tau_{relax}} = 0.9672$) and coloring values equal to $(n \pm 0.1)$ red, where n is an integer; the red values correspond to potential shapes where the natural frequency of the static potential is resonant with the oscillation frequency. This simulation approximately reproduces the interference-like patterns in the plots in **Figure 2**.

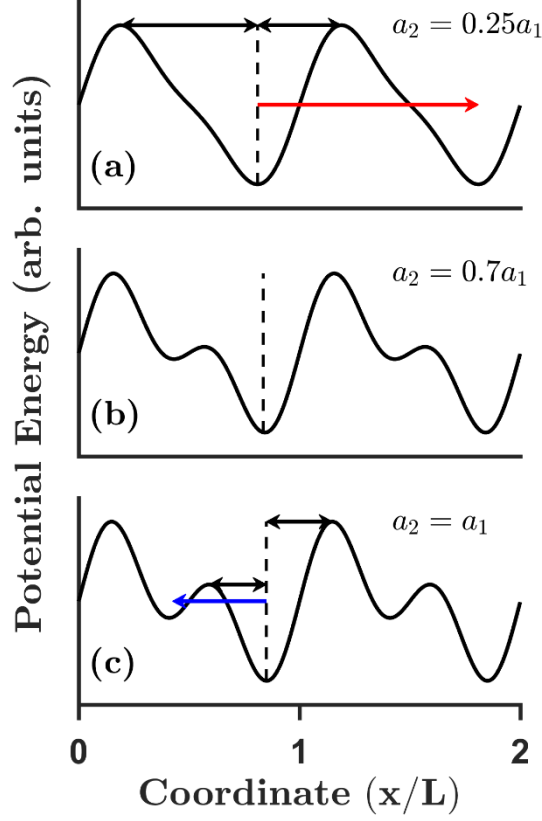


Figure 5. Representative potential shapes that lead to positive current (panel **a**, $a_2 = 0.25a_1$), zero current (panel **b**, $a_2 = 0.7a_1$), and negative current (panel **c**, $a_2 = a_1$) for “slow” ratchets, i.e., $\frac{\tau_{ratchet}}{\tau_{relax}} > 2.42$. In panel **a**, the current direction (red single arrow) is the shorter of two distances between a well and its two neighboring peaks, indicated by the double arrows. As a_2 becomes greater than $0.5a_1$, the shoulder transitions into a well (panel **b**). When a_2 is equal to larger than a_1 (panel **c**), the distance between the deepest well and its two neighboring peaks becomes very similar (compare black double arrows), and the asymmetry in the heights of those peaks controls the direction of current (blue single arrow). The maximum negative current we observe is smaller in magnitude than the maximum positive current we observe because trapping of the electron in the secondary well, which only occurs for scenarios like that in panel **c**, re-randomizes the direction of the current, as explained in the text.

REFERENCES

- [1] O. Hod and E. Rabani, Proc. Natl. Acad. Sci. U. S. A. **100**, 14661 (2003).
- [2] R. D. Astumian, Phys. Chem. Chem. Phys. **9**, 5067 (2007).
- [3] J. Rousselet, L. Salome, A. Ajdari, and J. Prost, Nature **370**, 446 (1994).
- [4] J. S. Bader, R. W. Hammond, S. A. Henck, M. W. Deem, G. A. McDermott, J. M. Bustillo, J. W. Simpson, G. T. Mulhern, and J. M. Rothberg, Proc. Natl. Acad. Sci. U. S. A. **96**, 13165 (1999).
- [5] P. Hänggi and F. Marchesoni, Rev. Mod. Phys. **81**, 387 (2009).
- [6] A. Auge, A. Weddemann, F. Wittbracht, and A. Hütten, Appl. Phys. Lett. **94**, 183507 (2009).
- [7] W. C. Germs, E. M. Roeling, L. J. van Ijzendoorn, B. Smalbrugge, T. de Vries, E. J. Geluk, R. A. Janssen, and M. Kemerink, Phys. Rev. E **86**, 041106 (2012).
- [8] A. M. Drews, H. Y. Lee, and K. J. Bishop, Lab Chip **13**, 4295 (2013).
- [9] M. Kabir, D. Unluer, L. Li, A. W. Ghosh, and M. R. Stan, Nanotechnology (IEEE-NANO), 2011 11th IEEE Conference on, 482 (2011).
- [10] M. Kabir, D. Unluer, L. Li, A. W. Ghosh, and M. R. Stan, IEEE T. Nanotechnol. **12**, 330 (2013).
- [11] E. M. Roeling, W. C. Germs, B. Smalbrugge, E. J. Geluk, T. de Vries, R. A. Janssen, and M. Kemerink, Nat. Mater. **10**, 51 (2011).
- [12] T. Tanaka, Y. Nakano, and S. Kasai, Jpn. J. Appl. Phys. **52**, 06GE07 (2013).
- [13] Y. Abe, R. Kuroda, X. Ying, M. Sato, T. Tanaka, and S. Kasai, Jpn. J. Appl. Phys. **54**, 06FG02 (2015).
- [14] H. Linke, T. E. Humphrey, A. Löfgren, A. O. Sushkov, R. Newbury, R. P. Taylor, and P. Omling, Science **286**, 2314 (1999).
- [15] A. M. Song, P. Omling, L. Samuelson, W. Seifert, I. Shorubalko, and H. Zirath, Appl. Phys. Lett. **79**, 1357 (2001).
- [16] A. M. Song, Appl. Phys. A: Mater. Sci. Process. **75**, 229 (2002).
- [17] S. Sassine, Y. Krupko, J. C. Portal, Z. D. Kvon, R. Murali, K. P. Martin, G. Hill, and A. D. Wieck, Phys. Rev. B **78**, 045431 (2008).
- [18] C. Drexler *et al.*, Nat. Nanotechnol. **8**, 104 (2013).
- [19] P. Reimann, M. Grifoni, and P. Hänggi, Phys. Rev. Lett. **79**, 10 (1997).
- [20] P. Reimann, Phys. Rep. **361**, 57 (2002).
- [21] R. Bartussek, P. Hänggi, and J. G. Kissner, Europhys. Lett. **28**, 459 (1994).
- [22] M. O. Magnasco, Phys. Rev. Lett. **71**, 1477 (1993).
- [23] A. Celestino, C. Manchein, H. A. Albuquerque, and M. W. Beims, Phys. Rev. Lett. **106**, 234101 (2011).
- [24] A. Celestino, C. Manchein, H. A. Albuquerque, and M. W. Beims, Commun. Nonlinear. Sci. **19**, 139 (2014).
- [25] L. Ermann and G. G. Carlo, Phys. Rev. E **91**, 010903 (2015).
- [26] M. W. Beims, M. Schlesinger, C. Manchein, A. Celestino, A. Pernice, and W. T. Strunz, Phys. Rev. E **91**, 052908 (2015).
- [27] G. G. Carlo, A. M. F. Rivas, and M. E. Spina, Phys. Rev. E **92**, 052907 (2015).
- [28] J. F. Chauwin, A. Ajdari, and J. Prost, Europhys. Lett. **32**, 699 (1995).
- [29] Y. D. Chen, B. Yan, and R. M. Miura, Phys. Rev. E **60**, 3771 (1999).
- [30] M. Kostur and J. Luczka, Phys. Rev. E **63**, 021101 (2001).

- [31] V. M. Rozenbaum, T. Y. Korochkova, D. Y. Yang, S. H. Lin, and T. Y. Tsong, *Phys. Rev. E* **71**, 041102 (2005).
- [32] J. Chacko and G. Tripathy, *Indian J. Phys.* **89**, 981 (2015).
- [33] E. M. Roeling, W. C. Germs, B. Smalbrugge, E. J. Geluk, T. de Vries, R. A. J. Janssen, and M. Kemerink, *AIP Adv.* **2**, 012106 (2012).
- [34] J. S. Roth, Y. Zhang, P. Bao, M. R. Cheetham, X. Han, and S. D. Evans, *Appl. Phys. Lett.* **106**, 183703 (2015).
- [35] A. J. Leggett, S. Chakravarty, A. T. Dorsey, M. P. A. Fisher, A. Garg, and W. Zwerger, *Rev. Mod. Phys.* **59**, 1 (1987).
- [36] L. Diosi, *Europhys. Lett.* **22**, 1 (1993).
- [37] S. Gao, *Phys. Rev. Lett.* **79**, 3101 (1997).
- [38] M. A. Schlosshauer, *Decoherence and the Quantum-To-Classical Transition* (Springer, Leipzig, 2008), The Frontiers Collection.
- [39] See Supplemental Material at [URL will be inserted by publisher] for data the shows the behavior of the ratchet model for different initial conditions, spatial periods, temperatures, and friction coefficients. Movies detailing the dynamics of the wavefunction are also included.
- [40] M. Berman and R. Kosloff, *Comput. Phys. Commun.* **63**, 1 (1991).
- [41] H. Chen, Q. Wang, and Z. Zheng, *Phys. Rev. E* **71**, 031102 (2005).
- [42] V. Kharchenko and I. Goychuk, *New J. Phys.* **14**, 043042 (2012).
- [43] J. Lehmann, S. Kohler, P. Hanggi, and A. Nitzan, *Phys. Rev. Lett.* **88**, 228305 (2002).
- [44] S. Denisov, L. Morales-Molina, S. Flach, and P. Hänggi, *Phys. Rev. A* **75**, 063424 (2007).
- [45] T. Salger, S. Kling, T. Hecking, C. Geckeler, L. Morales-Molina, and M. Weitz, *Science* **326**, 1241 (2009).
- [46] M. Heimsoth, C. E. Creffield, and F. Sols, *Phys. Rev. A* **82**, 023607 (2010).
- [47] F. Zhan, S. Denisov, A. V. Ponomarev, and P. Hänggi, *Phys. Rev. A* **84**, 043617 (2011).
- [48] C. Grossert, M. Leder, S. Denisov, P. Hanggi, and M. Weitz, *Nat. Commun.* **7**, 10440 (2016).
- [49] M. B. Tarlie and R. D. Astumian, *Proc. Natl. Acad. Sci. U. S. A.* **95**, 2039 (1998).
- [50] A. Kato and Y. Tanimura, *J. Phys. Chem. B* **117**, 13132 (2013).
- [51] V. Giannini, A. I. Fernández-Domínguez, S. C. Heck, and S. A. Maier, *Chem. Rev.* **111**, 3888 (2011).